Challenges in underwater navigation: exploring magnetic sensors anomaly sensing and navigation

Vladimir Djapic[1], Wenjie Dong[2], Adi Bulsara[1], and Greg Anderson[1]
[1]SPAWAR Systems Center Pacific, San Diego, CA,
[2]Department of Electrical Engineering, The University of Texas-Pan American, Edinburg, TX

***Abstract*— This work combines magnetic field sensing and underwater navigation without the need of a priori maps. The initial work utilizes distributed cooperative localization and control used estimate the states of nodes (autonomous underwater vehicles - AUVs) that carry magnetic sensors. Because of their size, weight, power consumption, and cost fluxgate magnetometers are considered. The distributed estimation method and formation control algorithms allow for the creation of various shapes (vertical, horizontal, and longitudinal) of gradiometer sensor using multiple gliders/AUVs that each carry magnetometers as opposed to traditionally considered arrays on a single AUV. This procedure can be applied in Mine Countermeasures (MCM) - military or unexploded ordnances (UXO) both to detect / localize the anomalies (mines) or cable and pipeline survey - civilian, thus serving as a "payload" sensor. At the same time, the same anomailes can be used as features for navigation corrections.**

I. Introduction

It is well know fact that high performance inertial navigation systems imply high cost. Military grade inertial measurement units (IMUs) used in, for example, submarines can cost over $ 1 M. Navigation grade IMUs used in commercial airplanes or in high end autonomous underwater vehicles (AUVs) cost on the order of $ 100 K. The precision of un-aided (without an absolute positioning system such as GPS) inertial navigation goes hand in hand with the price as high end military typically have position drifts of 1 nmi per day vs. 1 nmi per hour exhibited by the navigation grade ones. Typical Micro electromechanical systems (MEMS) IMUs that cost a few thousand dollars or less will drift at significantly higher rates (>10 nmi/hr). However, more advanced MEMS IMUs are nowdays alternatives to the older mechanical inertial sensors due to the significantly smaller cost, reduced size and power requirements but comparable performance. For example, gyro bias of 1 or 3 °/hr and even in some cases 0.5 °/hr is a reality for a bit more expensive ($ 10 K) MEMS IMUs. Gyro biases can be estimated by modern navigation software solutions but angle random walk, in some new units, of 0.02 $°/\sqrt[2]{h}$ is just an order of magnitude worse than navigation grade fiber optic or laser ring gyros (0.002 $°/\sqrt[2]{h}$). Also, fiber and laser tactical units are typically 10-20 cm boxes that weight of 2-5 kg while MEMS units are usually 2-5 cm^3 that weight <50 g. Because of these cost, size, weight, power requirements characteristics the goal is to incorporate new MEMS IMUs in the next generation AUVs.

Commercial off-the-shelf (COTS) AUVs are equipped with more costly sensors such as Doppler Velocity Log (DVL), and/or fiber optic / laser ring / MEMS IMU, and/or forward looking sonars. DVL measures speed over ground (underwater odometry) and is the main sensor for accurate underwater navigation of robots. IMU measures linear accelerations and angular rates. The aiding sensors include the DVL, external acoustic positioning system that are linked with the GPS system (long baseline - LBL or ultra-short baseline - USBL), pressure sensor, and usually a magnetic compass. Integration of the vehicles high-rate IMUs accelerometers and gyros allows time propagation while other low-rate sensors provide measurement corrections and this is done with the Kalman filter.

A good overview that explains different methods for underwater navigation is given in [8]. Their conclusion is that magnetic navigation can be useful if used in conjunction with other methods, for example bathymetric / altimeter sensors as an alternative to GPS aiding. An early work on exploring magnetic navigation for AUVs is presented in [9]. The author states that the fluxgate magnetometers with sensitivities of 10^{-11} Tesla can be used. In [10] triple redundancy navigation system incorporating magnetometer, inertial, and GPS measurements is presented. The recent technological advances offer many new possibilities for the compact, lightweight, inexpensive, low power both IMUs and magnetic sensors. More recently, [7] the utility of magentic sensing (passive and economical in terms of energy) vs. acoustic / sonar sensing (active, more power hungry and costly). As in [4] where the use of vector magnetic gradiometer on autonomous underwater vehicles has been explored for unexploded ordinances (UXO) detection we also want to explore the magnetometers as AUV "payload" sensors. The novelty of the approach presented here is having the baseline between the magnetometers extended using several AUVs flying in formation.

Section II explains our Distributed Kalman Filtering

978-1-4799-6117-7/15/$31.00 ©2015 IEEE

cooperative estimation, Section III describes sensor that is considered, magnetic anomaly detection, and magnetic navigation approaches, Section IV describes the results from the previous represenative experiments, and in Section V some future research goals are mentioned.

II. Distributed Kalman Filtering

Cooperation of multiple vehicles receive more attention in recent years as group performances can possibly lead to higher efficiency, robustness, and greater aperture. As opposed to centralized formation tracking control, distributed formation tracking control utilizes information of vehicle's own states and that from its neighbors. We will consider delayed communication for the proposed distributed controllers, estimate parameter uncertainties by adaptive control methods, and design a dynamics-based controller with the aid of kinematic-based controller and backstepping methods. For a COTS glider/AUV there are less control inputs than the numbers of the degree of freedom and control of it is challenging due to its underactuated nature and disturbances such as currents. In [2] the algorithms were presented that will be used for formation control of multiple glider/AUVs with uncertainty. It is assumed that there is parametric uncertainty and non-parametric uncertainty in the model of each glider/AUVs and the information of the leader glider/AUVs is available only to a portion of the follower glider/AUVs.

Distributed estimation with the aid of local information is challenging because information is not available for each agent. For multiple underwater vehicles with communication among vehicles, state estimation is more challenging because of limited communication bandwidth. In this paper, the new distributed estimation algorithms with the aid of Kalman filtering theory and distributed control theory are proposed.

A. Distributed Estimation for Static System

For a static system with state x, there are m agents which can measure an output of the system by the equipped sensors. For agent j, the measured output of the system is

$$y_j(k) = H_j x + v_j(k) \tag{1}$$

where H_j is the output matrix and v_j is the measurement noise. It is reasonable to assume that the measurement noise v_j is independent for different time and the measurement noise for different agents are independent, i.e.,

$$E[v_j(k)v_j^\top(l)] = R_j\delta_{kl} \tag{2}$$
$$E[v_j(k)v_i^\top(l)] = 0 \tag{3}$$

for any time k and l and for any $1 \le j \ne i \le m$, where R_j is a positive definite matrix.

For the m agents, the communication among agents is assumed. Each agent is considered as a node. The communication at time k can be defined by a directed graph $\mathcal{G}_k = \{\mathcal{A}, \mathcal{E}_k\}$ where $\mathcal{A}$ denotes the node set and $\mathcal{E}_k$ denotes the directed edges between nodes at time k. For agent j, its neighbors are in a set denoted by $\mathcal{N}_j$. The agent j and its neighbors are in a set denoted by $\bar{\mathcal{N}}_j$. It is obvious that $\bar{\mathcal{N}}_j = \mathcal{N}_j \cup \{j\}$.

For the communication graph, the following assumption is made.

Assumption 1: There exists a positive integer N such that the graph $(\mathcal{V}, \cup_{l=1}^{N}\mathcal{E}_{k+l})$ is strongly connected for all k.

For agent j, the cost function is defined as

$$J_j(k) = v_j^\top(k)R_j^{-1}v_j(k) \tag{4}$$
$$= (y_j(k) - H_j x)^\top R_j^{-1}(y_j(k) - H_j x) \tag{5}$$

The cost function at time k for all agents is defined as

$$J(k) = \sum_{j=1}^{m} J_j(k). \tag{6}$$

The distributed optimization problem of (6) with the aid of neighbors' information is solved.

With the aid of the results in [6], the estimate of x for agent j is

$$x_j(k+1) = \sum_{i\in\mathcal{N}_j} a_{ji}(k+1)x_i(k) - \alpha(k+1)H_j^\top R_j^{-1}(y_j(k+1) - H_j x_j(k)) \tag{7}$$

where $a_{ji}(k+1)$ are positive weights and $\alpha(k+1)$ is the stepsize.

For the stepsize, the following assumption is made.

Assumption 2: The stepsize sequence $\{\alpha(k)\}$ is non-negative, non-increasing, and such that

$$\sum_{k=1}^{\infty}\alpha(k) < \infty, \quad \sum_{k=1}^{\infty}\alpha(k)^2 < \infty$$

For the weights $\{a_{ji}\}$, the following assumption is made.

Assumption 3: For $i \in \mathcal{V}$ and all time k,

(a) $a_{ji}(k+1) \ge 0$, and $a_{ji}(k+1) = 0$ when $i \notin \mathcal{N}_j(k+1)$,

(b) $\sum_{i=1}^{m} a_{ji}(k+1) = 1$,

(c) There exists a scalar $\epsilon \in (0,1)$ such that $a_{ji}(k+1) \ge \epsilon$ when $i \in \mathcal{N}_j(k+1)$,

(d) $\sum_{j=1}^{m} a_{ji}(k+1) = 1$.

For the algorithm (7), the following results are obtained.

Theorem 1: Let Assumptions 1-3 hold, the estimate (7) ensures that

$$\lim_{k\to\infty} \|x_j(k) - x^*\| = 0 \tag{8}$$

for $1 \leq j \leq m$, where x^* is the solution of the minimization problem (6).

Theorem 1 can be proved by following the proof in [6] and is omitted here for space limit.

B. Distributed Estimation of Dynamic System

For a linear dynamic system

$$x(k+1) = A(k)x(k) + w(k) \tag{9}$$

where $x(k)$ is the state and $w(k)$ is the noise. It is assumed that

$$E(w(k)) = 0, \quad E(w(k)w(l)^\top) = Q\delta_{kl}$$

where Q is a positive definite matrix.

There are m agents which can measure an output of the system by the equipped sensors. For agent j, the measured output of the system is (1), where H_j is the output matrix and v_j is the measurement noise. It is reasonable to assume that the measurement noise v_j is independent for different time and the measurement noise for different agents are independent, i.e., (2)-(3) are satisfied for positive definite matrix R_j. The communication digraph at time k is defined by a digraph $\mathcal{G}(k) = \{\mathcal{A}, \mathcal{E}(k)\}$.

An estimate $x(k)$ for agent j is found such that the cost function in (6) is minimized in two steps.

Step 1: At time $k+1$, if there is no measurement available the estimate of $x(k+1)$ is denoted as $x_j^-(k+1)$. Taking the expectation of both sides of (9) results in

$$E(x(k+1)) = A(k)E(x(k))$$

Therefore, the unbiased state estimate at time $k+1$ prior to incorporating the measurement is

$$x_j^-(k+1) = A(k)x_j^+(k) = x(k+1) - x_j^-(k+1) \tag{10}$$

The variance of this estimate is

$$\begin{aligned} P_j^-(k+1) &= Var(\tilde{x}_j^-(k+1)) \\ &= Var((x(k+1) - x_j^-(k+1)) \\ &= A(k)P_j^+(k)A^\top(k) + Q_k \end{aligned}$$

Step 2: At time $k+1$, there is measurement y_{k+1} and $x(k+1)$ is estimated based on the following two sets of information

$$\begin{aligned} x_j^-(k+1) &= x(k+1) - \tilde{x}_j^-(k+1) && (11) \\ y_j(k+1) &= H_j x(k+1) + v_j(k+1) && (12) \end{aligned}$$

where $Var(\tilde{x}_j^-(k+1)) = P_j^-(k+1)$, $Var(v_j(k+1)) = R_j$, $\tilde{x}_j^-(k+1)$ and $v_j(k+1)$ are linearly independent.

For agent j, the cost function is defined as

$$\begin{aligned} J_j(k+1) = v_j(k+1)^\top R_j^{-1} v_j(k+1) \\ +(\tilde{x}_j^-(k+1))^\top (P_j^-(k+1))^{-1} \tilde{x}_j^-(k+1) \end{aligned} \tag{13}$$

For all agents, the cost function is defined as

$$J(k+1) = \sum_{j=1}^{m} J_j(k+1) \tag{14}$$

The minimization problem of (14) is solved and the following estimate algorithm is proposed as

$$\begin{aligned} x_j^+(k+1) = \sum_{i\in\bar{\mathcal{N}}_j(k+1)} a_{ji}(k+1)x_i^+(k) \\ -\alpha(k+1)H_j^\top R_j^{-1}(y_j(k+1) - H_j x_j^-(k+1)) \end{aligned} \tag{15}$$

For the algorithm (10) and (15), the following results are obtained.

Theorem 2: Let Assumptions 1-3 hold, the estimate (10) and (15) ensures that

$$\lim_{k\to\infty} \|x_j(k) - x^*(k)\| = 0 \tag{16}$$

for $1 \leq j \leq m$, where x^* is the solution of the minimization problem (14).

Theorem 2 is a summary of the work in Step 1 and step 2. It can be proved with the aid of Theorem 1 and is omitted here.

It should be noted that in the algorithm (15) the variance of the estimation is not taken into consideration. In order to take the advantage of the variance of the estimation, the Theorem 2 is refined.

The algorithm (15) can be written as

$$\begin{aligned} x_j^+(k+1) = \sum_{i\in\bar{\mathcal{N}}_j(k+1)} a_{ji}(k+1)x_i^+(k) \\ -\alpha(k+1)H_j^\top R_j^{-1}(H_j x(k+1) \\ -H_j x_j^-(k+1) + v_j(k+1)) \end{aligned} \tag{17}$$

The variance of $x_j^+(k+1)$ can be calculated as follows.

$$P_j^+(k+1) = \sum_{i\in\bar{\mathcal{N}}_j(k+1)} a_{ji}^2(k+1)P_i^+(k)$$
$$+\alpha(k+1)^2 H_j^\top R_j^{-1} H_j P_j^-(k+1) H_j^\top R_j^{-1} H_j$$
$$+\alpha(k+1)^2 H_j^\top R_j^{-1} H_j \quad (18)$$

Parameter a_{ji} is chosen as a function of the variance of the estimation at each step and propose the following results.

Theorem 3: Let Assumptions 1-3 hold, the estimate (10) and (15) ensures that

$$\lim_{k\to\infty} \|x_j(k) - x^*(k)\| = 0 \quad (19)$$

for $1 \le j \le m$, where x^* is the solution of the minimization problem (14), a_{ji} is defined as

$$a_{ji}(k+1) = \max\left\{\frac{P_i^+(k)}{\sum_{l\in\bar{\mathcal{N}}_j(k+1)} P_l^+(k)}, \epsilon\right\},$$
$$i \in \bar{\mathcal{N}}_j(k+1). \quad (20)$$

With a_{ji} defined in (20), Assumption 3 is satisfied. By Theorem 2, the claims in Theorem 3 are correct.

In summary, the following algorithm is proposed.

Predict:

Predicted (a priori) state estimate: $x_j^-(k+1) = A(k)x_j^+(k)$

Predicted (a priori) estimate covariance: $P_j^-(k+1) = A(k)P_j^+(k)A^\top(k) + Q_k$

Update:

Updated (a posteriori) state estimate:

$$x_j^+(k+1) = \sum_{i\in\bar{\mathcal{N}}_j(k+1)} a_{ji}(k+1)x_i^+(k)$$
$$-\alpha(k+1)H_j^\top R_j^{-1}(y_j(k+1) - H_j x_j^-(k+1))$$

Updated (a posteriori) estimate covariance:

$$P_j^+(k+1) = \sum_{i\in\bar{\mathcal{N}}_j(k+1)} a_{ji}^2(k+1)P_i^+(k)$$
$$+\alpha(k+1)^2 H_j^\top R_j^{-1} H_j P_j^-(k+1) H_j^\top R_j^{-1} H_j$$
$$+\alpha(k+1)^2 H_j^\top R_j^{-1} H_j$$

C. Applications of the Proposed Algorithms

We consider multiple vehicles where each vehicle is equipped with different sensors. The dynamics of vehicle j is

$$\dot{z}_j = f_j(z_j, v_j) \quad (21)$$

where z_j is the state and the noise of the vehicle.

The state of each vehicle with the aid of its own sensors and its neighbors' information should be estimated. To this end, (21) is converted to discrete time. Its discrete-time model can be written as

$$z_j((k+1)T) = \Phi_j(kT)z_j(kT) + B_j(kT)v_j(kT)$$

Let $x(k) = [z_1^\top(kT), \ldots, z_m^\top(kT)]^\top$ and $w(k) = [(B_1(kT)v_1(kT))^\top, \ldots, (B_m(kT)v_m(kT))^\top]^\top$, the dynamics of the m systems can be written as (9), where $A(k) = \mathrm{diag}[\Phi_1(kT), \ldots, \Phi_m(kT)]$. The sensor's measurement of vehicle j can be written as (12) by linearization.

The algorithm is applied in the subsection II-B to estimate $x(k)$ for each vehicle. Therefore, each vehicle can estimate its own state.

III. Sensor, Magnetic anomaly detection, Magnetic Navigation

In general there are two types of magnetometers - total (measure the magnitude of the magnetic field but not its direction) and vector (measure both) field. Vector magnetometers include fluxgate (can usually measure between 10^{-2} T and 10^{-10} T but they can reach 10^{-11} T resolution) and superconducting quantum interference device (SQUID).

The SSC Pacific (SSC)'s fluxgate magnetometer presented here is a hockey puck-sized sensor head that can detect vehicles, weapons, or other targets by measuring changes in the magnetic field caused by movements of ferro-magnetic material in the vicinity of the sensor. SSC has developed and built two kinds: Single-core fluxgate (SCFG) and Coupled-core fluxgate (CCFG). Both SCFG and CCFG version exploits nonlinear dynamic phenomena to yield significantly enhanced sensitivity. For example, resolution of SCFG was improved from to 8x10^{-10} T to 1.1x10^{-10} T by optimization of the readout circuit.

The fluxgate magnetometer consists of two coils, "excitation" and "pickup" coil. In the presence of a time-periodic, sinusoidal bias signal $h(t)$ and without any external magnetic field, the flux in one core half cancels that in the other, and the output voltage V_0 at the "pickup" coil will be alternating and symmetric in time (shown in Fig. 1 - above, target signals $H_x = 0$, threshold bias signal H_e or $-H_e$ crossings time is equal, $T^+ = T^-$). An external magnetic field, caused by a target signals,H_x, will shift the sinusoidal signal upward by an amount H_x (shown in Fig. 1 - below, target signals $H_x > 0$, threshold bias signal H_e or $-H_e$ crossings time is not equal, $T^+ \neq T^-$)). Thus, residence times difference (RTD) can be used to determine the strength of the target signals using fluxgate magnetometers as

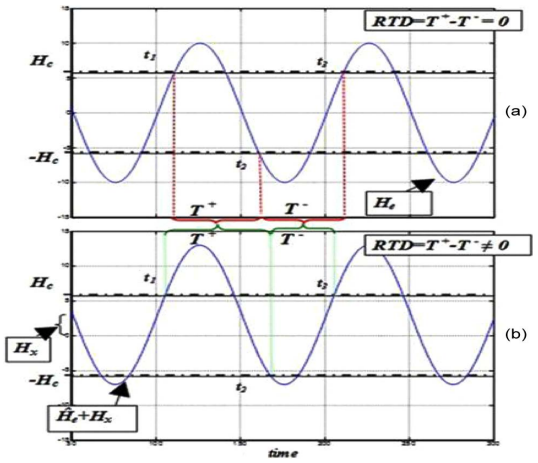

Fig. 1: RTD readout scheme.

explained in [1]. The important point is that, in the RTD approach, events (corresponding to threshold crossings) are considered rather than signal amplitudes (as necessary in a conventional PSD-based readout). This approach leads to an extremely simple readout circuitry, mainly based on a fast clock and counterkeeping a running arithmetic mean (necessary when a noise floor is present) of the RTD. In addition, many noise effects are also mitigated by the intrinsic decoupling between the amplitude domain of the input signal and the event or time domain of the output signal.

Just from one author [5], numerous patents exist: 1) to classify underwater buried mine with scalar magnetometers, 2) to deploy magnetic marker to fix AUV position using a triaxial vector magnetometer in which the magnetic sensors are mutually orthogonal and IMU data, 3) a system for passively measuring the AUV velocity using two biaxial fluxgate magnetometers separated by a known distance and oriented precisely with respect to one another and with respect to the path of travel, and 4) a navigation system for navigating underwater a killer vehicle towards a mine by two magnetic sensors. Similarly, the plan is to use magnetic sensing, together with some other inexpensive senors, for final homing / attachment on the magnetic mine to augment approach presented here (uses another surface or underwater robot that provides navigation aiding to the mine killer vehicle via onboard sonar) presented in [3] which proved to be very robust solution to get within the final homing range. All of these patent have some things in common with approach presented in this paper: inertial navigation sensor, and two or more magnetometers vs. one can improve performance. The approach is to use the advances in MEMS IMU and fluxgate designs and separate the magnetometers (therefore increase the baseline) on two or more AUVs.

For the initial test, two SCFG magnetometers are being integrated onto a Slocum glider made by Teledyne Web Research. Fig. 2 shows the glider with two ”extra” fins that contain SCFG with the CAD model shown in Fig. 3. Wave-Adaptive Modular Vessel (WAM-V) Unmanned Surface Vehicle, developed by Marine Advanced Research, Inc., shown in Fig. 4, will be used to tow the glider / magnetometer system. The mission that will be performed is the system executing autonomous search patern in the artificial mine field.

IV. Previous Representative Experiments

In this paper two, out of many, experiments (underwater and ground) done with SSC's SCFG are presented. Both experiments are representative of the missions that will be tested in future.

An array of seven SCFG sensors on the bay floor (separated by the distance of 4.5 meters) were tested in counter swimmer test in Aug 2006. Two swimmers separated by short distances were instructed to pass 4.5 meters above the bottom. Fig. 5 shows the output of each of the seven SCFG where two blips indicate detection of both swimmers. In Fig. 6 the output signal measured from two swimmers one behind the other is shown: in this case two blips can be observed in the output signal, corresponding to multiple intrusion, track perfectly the swimmers in both directions. Predicted (theoretical) detection range for swimmer with commercial gear and a small weapon is about 12 m with 2x10^{-10} T resolution sensor - current lab version of CCFG which leads us to the conclusion that these sensor can me used in MCM and UXO detection missions.

An experiment that was done in 2007 shows representative results of using two SCFG magnetometers as gradiometers for detection of passenger cars passing by with the purpose of testing if vehicle direction could be determined by the delay in the peak signal. A pair of SCFG magnetometers were spaced about 2 m apart parallel to the street, about 11.3 m from the center of the street and the cars were from 10 to 17 m away, depending on which side of the street they were driving. The output is at about a 10 Hz rate, with each data point representing the change in the magnetic field from a base line calculated from a 10 second moving average. The residence time diference (RTD) was measured by which the detection of the magnetic field resides in time rather than in amplitude. In the detection algorithm used the 32 point moving average background is subtracted from the average of the 8 most recent samples (about .46 seconds of data). This effectively filters out the high and low frequency signals outside the range of interest for a moving vehicle. The transients in the local magnetic field caused by the passing of the car are detected. This magnetometer used a a couple of counters clocked at

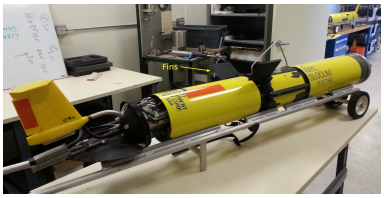

Fig. 2: Slocum glider with fins (SCFG).

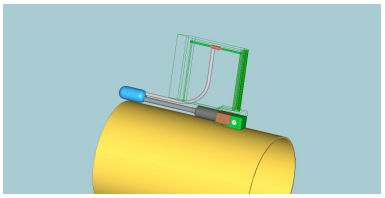

Fig. 3: SCFG fin design.

Fig. 4: WAM-V USV.

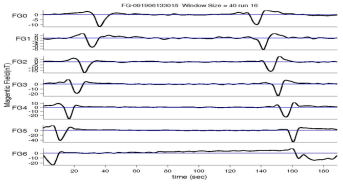

Fig. 5: the output of each of the seven fluxgates used.

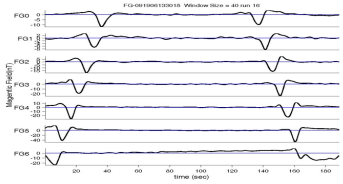

Fig. 6: the output signal measured from two swimmers one behind the other.

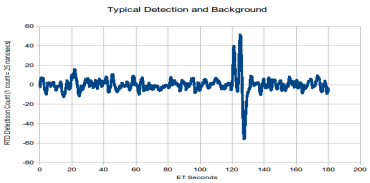

Fig. 7: Typical detection of a car by SCFG.

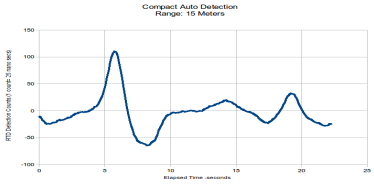

Fig. 8: Detection of a car from 15 m.

Fig. 9: Image of a car passing.

Sensor	Manufacturer	Type	Quoted Noise Floor (pT / rt Hz)	Tested Noise Floor	Approximate Cost	Notes
Mag648	Bartington	Fluxgate - Vector	10 @ 1 Hz	Untested by SSC		
DFM28G	Billingsley	Fluxgate - Vector	8 @ 1 Hz	40 @ 1 Hz	8K	
Overhauser	Marine Magnetics	Overhauser - Scalar	10 @ 1 mHz	100 @ 1 mHz	20K	
He3	Polatomic	Nuclear Precession - Scalar	1 @ 4 mHz	4 @ 4 mHz	75K	Bench Top Testing - not achievable at-sea.
He4	Polatomic	Nuclear Precession - Vector	1 @ 4 mHz	Untested by SSC	100K+	Continuously laser pumped. Requires power source.
Single Core	SSC Pacific	Fluxgate - Vector 2 Channels		100 @ 1 Hz	< 0.8K	
Coupled Core	SSC Pacific	Fluxgate - Vector 3 Channels		50 @ 1 Hz	< 1K	

Fig. 10: Comparison of various magnetometers.

40MHz so each count was 1/40MHz or 25 nanoseconds of RTD. One counter tracks the time the "pickup" coil output is above zero volts and the other counter tracks the time the output is below zero volts. Fig. 7 shows a typical, very clear signal when a car is detected at the distances on the order of 15 m. Fig. 8 shows the zoomed in detection (peak of 100 counts which is 2500 nanoseconds RTD) of a car passing by which is shown in Fig. 9.

V. Conclusion

The possibilities offered by new technologies and materials in realizing MEMS devices with improved performance have led to great interest in a new generation of inexpenisve, compact, and low-power IMU, magnetometer, and e-field sensors - which are also being developed. In Fig. 10 a comparison table of SCC's SCFG and CCFG with similar COTS magnetometers is shown. New underwater sensing techniques when combined with cooperative decentralized localization, navigation, and control algorithms being developed for swarm mobile robots applications offer vast possibilities in adaptive sampling of the ocean. Even with the integration of Doppler velocity loggers (DVL) with INS to improve the performance of dead-reckoning navigation systems, the positioning error grows unbounded at a considerable rate and an alternative to GPS system for absolute positioning is desired.

References

[1] B. Ando, S. Baglio, A. Bulsara, and V. Sacco, "Residence times difference fluxgate magnetometers," IEEE Sensors J., vol. 5, no. 5, pp. 895904, Oct. 2005.

[2] Chen, C., Xing, Y., Djapic, V., Dong, W, "Distributed Formation Tracking Control of Multiple Mobile Robotic Systems", IEEE Conference on Decision and Control, 2014.

[3] Vladimir Djapic, Dula Nad, Gabriele Ferri, Edin Omerdic, Gerard Dooly, Dan Toal, Zoran Vukic, "Novel method for underwater navigation aiding using a companion underwater robot as a guiding platforms," OCEANS'13, Bergen, Norway, 2013.

[4] Pei, Y. H., and H. G. Yeo. "UXO survey using vector magnetic gradiometer on autonomous underwater vehicle." OCEANS, 2009.

[5] Donald Polvani' patents. http://patents.justia.com/inventor/donald-g-polvani.

[6] Sundhar Ram, S., Nedic, A., Veeravalli, V.V. "A new class of distributed optimization algorithms: application to regression of distributed data," Optimization Methods and Software, vol. 27, 2012.

[7] F.C. Teixeira, A. Pascoal. "Magnetic Navigation and Tracking of Underwater Vehicles." 9th IFAC Conference on Control Applications in Marine Systems, CAMS 2013. Osaka, Japan.

[8] Tuohy, S. T., Patrikalakis, N. M., Leonard, J. J., Bellingham, J. G., and Chryssostomidis, C., "AUV Navigation Using Geophysical Maps with Uncertainty," Proceedings 8th International Symposium on Unmanned, Untethered Submersible Technology, pp 265-276, 1993.

[9] Carl Tyren (1982), "Magnetic Anomalies as a Reference for Ground-speed and Map-matching Navigation. Journal of Navigation," 35, pp 242-254.

[10] Yang, Yunchun, and Jay A. Farrell. "Magnetometer and differential carrier phase GPS-aided INS for advanced vehicle control." Robotics and Automation, IEEE Transactions on 19.2 (2003): 269-282.